HHS Public Access

Author manuscript

Int J Hyperthermia. Author manuscript; available in PMC 2021 February 05.

Published in final edited form as:

Int J Hyperthermia. 2020 ; 37(1): 1189–1201. doi:10.1080/02656736.2020.1829103.

Feasibility of Removable Balloon Implant for Simultaneous Magnetic Nanoparticle Heating and HDR Brachytherapy of Brain Tumor Resection Cavities

Paul R. Stauffer[1,*], **Dario B. Rodrigues**[2], **Robert Goldstein**[3], **Thinh Nguyen**[1,4], **Yan Yu**[1], **Shuying Wan**[1], **Richard Woodward**[5], **Michael Gibbs**[5], **Ilya L Vasilchenko**[6], **Alexey M Osintsev**[7], **Voichita Bar-Ad**[1], **Dennis B. Leeper**[1], **Wenyin Shi**[1], **Kevin D. Judy**[8], **Mark D. Hurwitz**[1]

[1]Thomas Jefferson University, Radiation Oncology Dept., Philadelphia PA

[2]Univ. Maryland School of Medicine, Radiation Oncology, Baltimore MD

[3]AMF Life Systems, Auburn Hills, MI

[4]Drexel University, Biomedical Engineering Dept., Philadelphia PA

[5]BrachyThermix LLC, Voorhees, NJ

[6]Kemerovo Regional Clinical Oncology Center, Head and Neck Dept

[7]Kemerovo State University, General Physics Dept.

[8]Thomas Jefferson University, Neurosurgery Department

Abstract

Aim: Hyperthermia (HT) has been shown to improve clinical response to radiation therapy (RT) for cancer. Synergism is dramatically enhanced if HT and RT are combined simultaneously, but appropriate technology to apply treatments together does not exist. This study investigates the feasibility of delivering HT with RT to a 5-10mm annular rim of at-risk tissue around a tumor resection cavity using a temporary thermobrachytherapy (TBT) balloon implant.

Methods: A balloon catheter was designed to deliver radiation from High Dose Rate (HDR) brachytherapy concurrent with HT delivered by filling the balloon with magnetic nanoparticles (MNP) and immersing it in a radiofrequency magnetic field. Temperature distributions in brain around the TBT balloon were simulated with temperature dependent brain blood perfusion using numerical modeling. A magnetic induction system was constructed and used to produce rapid heating (>0.2°C/s) of MNP-filled balloons in brain tissue-equivalent phantoms by absorbing 0.5 W/ml from a 5.7 kA/m field at 133 kHz.

[*]Correspondence: paulrstauffer@gmail.com.

Disclosures of Interest

The authors declare no conflict of interest other than R.G. who is an employee of AMF Life Systems.

Patents

Thomas Jefferson University has patent pending technology with a published international patent application for treating tumor bed margins of a resection cavity with simultaneous heat and radiation (87). AMF Life Systems has patented technology for induction coils and systems for magnetic hyperthermia (35).

Results: Simulated treatment plans demonstrate the ability to heat at-risk tissue around a brain tumor resection cavity between 40-48°C for 2-5cm diameter balloons. Experimental thermal dosimetry verifies the expected rapid and spherically symmetric heating of brain phantom around the MNP-filled balloon at a magnetic field strength that has proven safe in previous clinical studies

Conclusions: These preclinical results demonstrate the feasibility of using a TBT balloon to deliver heat simultaneously with HDR brachytherapy to tumor bed around a brain tumor resection cavity, with significantly improved uniformity of heating over previous multi-catheter interstitial approaches. Considered along with results of previous clinical thermobrachytherapy trials, this new capability is expected to improve both survival and quality of life in patients with glioblastoma multiforme.

Graphical Abstract:

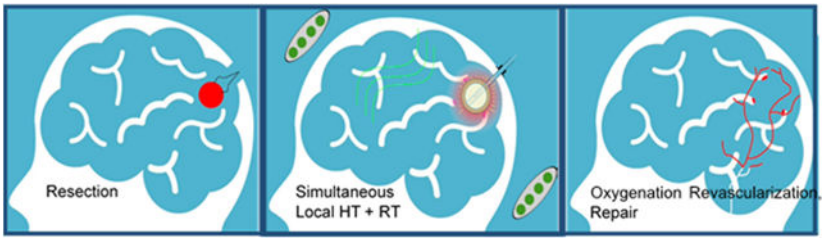

Keywords

Hyperthermia; thermobrachytherapy; nanoparticles; tumorbed therapy; cancer

1. Introduction

Surgery is a critical component of therapy for many cancer patients, but effective therapy often requires post-surgical treatment of micrometastatic deposits of tumor cells that infiltrate normal tissues around the resection cavity. Radiation therapy (RT) of the tumor bed improves clinical response, but RT dose is limited by normal tissue toxicity. For aggressive tumors like glioblastoma multiforme (GBM), external beam radiation (EBRT) is normally delivered in 5 day/week fractions over 6 weeks (1). Despite treatment that generally includes temozolomide (TMZ) chemotherapy, patients typically fail locally with median survival approximately 18 months for primary GBM and 12 months for recurrent GBM (2-7). Alternatively, there are approaches that localize higher doses of RT to at-risk tissues around the resection cavity by: a) temporarily implanting an array of catheters to insert radioactive seeds that deliver RT over 3-5 days; b) permanently implanting an array of short half-life RT seeds that deliver dose slowly over 4-5 weeks; or c) placing an inflatable balloon in the resection cavity at the time of surgery with a catheter exiting the skin for subsequent insertion of either a radioactive fluid or High Dose Rate (HDR) source to deliver radiation over 1-5 days before withdrawing the balloon. FDA-approved inflatable balloon medical devices have been developed to deliver brachytherapy in brain (8), breast (9, 10), and other sites. The current effort investigates a brachytherapy balloon implant that adds the capability of simultaneous thermal therapy to boost clinical outcomes in aggressive brain cancers.

Combining thermal therapy (40-48°C for 15-60 min) with radiation has been proven to enhance radiation response both *in vitro* and *in vivo* (11-13) as well as improve clinical outcomes in 24 positive randomized clinical trials (14, 15). Particularly relevant for brain tumor therapy is one randomized trial in primary GBM that demonstrated a statistically significant doubling of 2-year survival (31 vs. 15%, p=0.02) by adding two 30 min treatments with interstitial microwave hyperthermia to the then standard of care: regional brain RT + oral hydroxyurea + interstitial seed brachytherapy boost to tumor bed (16). A similar trial investigated adding thermotherapy via implanted ferromagnetic seeds to an EBRT + brachytherapy regimen and demonstrated a 47% 2-year survival in primary high-grade gliomas (17). The 31% and 47% 2-year survival rates obtained in these 1990's brain tumor trials remain among the best clinical outcomes for GBM to date, and clearly demonstrate the benefit of adjuvant hyperthermia even when not optimally delivered. Unfortunately, the university-developed heating technologies used in those two trials were never made available commercially and these promising thermoradiotherapy approaches could not be incorporated into clinical practice. Subsequently, a new approach for heating brain tumors was developed based on inductively heating magnetic nanoparticles that are injected via multiple needle tracks into the tumor volume. Using a commercially available magnetic induction system, clinical trials have demonstrated a median survival of 23.2 mo for primary GBM using nanoparticle heating in combination with fractionated stereotactic RT (18, 19). As additional rationale to accelerate use of adjuvant heat in treating GBM, we point to critically important preclinical *in vivo* murine studies that demonstrate a dramatic escalation of thermal enhancement ratio (TER) from 1.5 for sequential heat and radiation, as used in previous clinical studies, to 5.0 for simultaneous treatments (12, 13). The impact of increased synergism between HT and RT when delivered concomitantly and at higher thermal dose levels is that clinical response with adjuvant HT can be increased up to 5 times higher than with RT alone. Unfortunately, there is no commercially available technology to apply HT and RT simultaneously in human brain.

To address this need, our proposed approach is a straightforward combination of previous technology that should provide improved uniformity of both HT and RT dose around a tumor resection cavity as well as enable simultaneous delivery for maximum TER. To implement this treatment strategy, we will construct a dual-modality thermobrachytherapy (TBT) device from an inflatable balloon with catheters extending from the resection cavity outside the skull for insertion of HDR brachytherapy source, saline, magnetic nanoparticle (MNP) solution, and temperature sensor (see Figure 1). After surgical placement of the balloon catheter at time of tumor debulking, the inner balloon will be filled with saline to expand the resection cavity into approximately spherical shape. After magnetic resonance (MR) imaging for treatment planning, some of the saline will be replaced with an equivalent volume of MNP solution in the outer balloon and the central catheter connected to a commonly available HDR remote afterloader. The patient will sit or lie with their head inside a non-contacting induction coil that generates a magnetic field within the brain for ~30 min while HDR brachytherapy is administered from a source inserted to the balloon center. Simultaneous heat and brachytherapy will be administered in a single dose immediately after surgery, or the combination treatment repeated daily for up to a week before removal of the balloon under local anesthetic. The clinical consequence is a single

surgery implant that provides higher and more uniform radiation dose to a spherically symmetric tumor bed than alternative approaches, with simultaneous thermotherapy to enhance RT response locally while minimizing toxicity. The HDR source, MNP, and deflated balloon are easily withdrawn at the end of therapy to complete the intervention in ≤1 week. This procedure will reduce overall treatment time and cost, eliminate irradiation of surrounding normal tissue, and reduce neurocognitive deficit that often accompanies regional treatment of brain.

Optimum treatment of GBM remains a controversial subject. Clinical trials have investigated numerous combinations of external beam radiation, systemic chemotherapy (2, 20), focused stereotactic radiosurgery (21), local radiation boost to tumor bed via interstitial implant (22, 23), GammaTile therapy (24), local chemotherapy (e.g. carmustine or Gliadel® wafers) (25, 26), (16, 17, 19)and/or immunotherapy (27, 28). Additionally, several trials have investigated local hyperthermia as a means to enhance radiation response while minimizing peripheral normal tissue toxicity (16, 17, 19). Overall, median survival remains stubbornly under 24 months for primary GBM regardless of approach. Although some of the best 2-year survival results were reported in the 1990's by Sneed *et al.* (16) and Stea *et al.* (17) where they combined EBRT with systemic chemotherapy and local brachytherapy plus interstitial HT, neither investigator used FDA-approved heating technology and the promising investigations ended with the end of grant funding. After over 20 years, overall median survival for primary GBM remains lower than was obtained in those three hyperthermia trials even with advances such as improved radiation delivery, TMZ, and other targeted agents and immune boosts.

The primary goal of this effort is to demonstrate feasibility of a novel combination thermobrachytherapy balloon device that should facilitate new clinical trials to investigate simultaneous heat and radiation delivered uniformly and well-localized in tumor bed immediately after surgery, before tumor cell migration into surrounding normal brain. This initial study focuses on thermal performance of a TBT balloon since the dosimetry of HDR radiation from within an implanted balloon catheter source is already well-characterized in the literature for soft tissue sites including brain and breast (9, 29, 30). Subsequent *in vivo* studies and clinical trials with the proposed thermobrachytherapy device will be required to determine: a) optimum balloon temperature and penetration depth of therapy for brain; b) optimum brachytherapy dose for combined therapy; c) optimum fractionation of heat and brachytherapy; and c) whether combination strategies of thermobrachytherapy with EBRT, chemotherapy, temozolomide, and/or immunotherapy would be beneficial for GBM and other resected brain tumors.

2. Materials and Methods

2.1. Thermobrachytherapy Balloon Implant

The thermobrachytherapy (TBT) balloon design is illustrated in Figure 1. It will be fabricated from an FDA-approved extruded plastic shaft and molded balloons (in several diameters), and integrated with commercially available catheter materials. The dual-balloon design is proposed to enable inflation of the inner balloon with inexpensive saline to expand the resection cavity into approximately spherical shape and filling of the outer balloon with a

MNP solution that absorbs energy from an external magnetic field to generate heat. The MNP solution and magnetic field are homogenous, thus produce equal temperature of the balloon surface in contact with the wall of the resection cavity. In order to heat the entire tumor bed to a therapeutic temperature range of 40-48°C, a radiofrequency current will be driven through a non-contacting induction coil that encircles the head to couple energy into the MNP solution. Power will be adjusted to maintain balloon surface temperature at the prescribed therapeutic level, which is calculated during HT treatment planning and monitored during treatment with a fiberoptic temperature sensor in the outer balloon. During heating, a single HDR radiation source will be driven by a standard clinical remote afterloader to the center of the inner balloon to deliver radiation uniformly to the nearly spherical resection cavity wall. This simultaneous heat and radiation treatment will be repeated daily for up to one week post-surgery. After this treatment, the balloon will be deflated and the device retracted through the skin in a minor procedure with local anesthetic at the scalp exit point.

2.2. Magnetic Nanoparticles

Magnetic nanoparticles have been widely investigated for clinical applications ranging from contrast enhancement of MR imaging (31, 32) to hyperthermia therapy for cancer (33, 34). Iron oxide magnetic nanoparticles may be purchased from commercial suppliers such as Sigma-Aldrich Corp. (St. Louis, MO), Micromod Partikeltechnologie GmbH (Rostok, Germany), Nanocs Inc. (New York, NY), or others. Following preliminary power absorption studies with various formulations and iron concentrations, the nanoparticles chosen as optimum for the current investigation were obtained from Micromod Partikeltechnologie GmbH (Rostok, Germany) as Perimag-CR with 130 nm size and iron concentration of 17.1 mg/ml. The nanoparticles were prepared and bottled in a cleanroom according to EU GMP guidelines.

2.3. Magnetic Field Generating System

The experimental system used to activate the nanoparticle filled balloons consists of a 7.5 kW, 80-180 kHz induction heating system assembled with an elliptically shaped 26 × 31 × 20 cm^3 coil which is appropriately sized to accommodate the human head (AMF Life Systems, Auburn Hills MI). The system shown in Figure 2 was configured to produce a magnetic field strength in the range 1.9 - 8.1 kA/m at 133 kHz in the central volume of the coil. The coil length and elliptical dimensions, including protective housing, were optimized to produce a more uniform field well-matched to the human head for maximum differential power absorption in a nanoparticle-filled balloon relative to direct heating of brain tissue (35). Field uniformity within the coil was assessed with a 1 cm diameter magnetic field probe (AMF Life Systems, Auburn Hills MI) mapped in 1 cm increments along 43 axial tracks measuring field strength throughout the coil from end to end and from coil center to outer plastic casing.

2.4. Laboratory Measurement of Balloon Implant Heating

Rate of temperature rise tests were used to characterize power absorption in the nanoparticle fluid as a function of field strength. A fixed volume of nanoparticle fluid was placed in a test chamber in the center of the coil with magnetic field probe and temperature sensors

immediately adjacent to the fluid. To establish reproducibility of heating and stability of the MNP solution during heating, multiple independent experiments were performed at field strengths ranging from 4.6 - 8.1 kA/m over a period of 5 months, while storing the test solution in a refrigerator between heat experiments. Due to the lack of preferred fiberoptic thermometry, temperature monitoring for the heating rate studies was provided by a 16-channel Hioki Data Acquisition Device (Hioki USA, Cranbury NJ) with 40 gauge Type E thermocouples. Wires were oriented perpendicular to the magnetic field as possible to minimize interference on the readout. A field-dependent <2°C artifact was evident on the readout which remained constant throughout the heating period and thus did not affect heating rate calculations.

For more realistic modeling of balloon heating in a non-perfused thermal load, a split-apart, 3-D printed full size human head phantom was constructed and filled with TX-151 gel phantom with thermal conductivity similar to human brain white matter. A 2-cm diameter MNP-filled test balloon (GliaSite®) was inserted 3-5 cm deep in the brain/skull phantom and placed in the center of the induction coil (Figure 3). Temperatures were monitored with Type E thermocouples located 0, 2.5, 5, 7.5, 10 and 12.5 mm from the balloon surface during application of the magnetic field to characterize radial penetration of heating around the balloon. In a separate heating procedure with no internal thermocouple probes, the brain phantom was removed from the induction coil and the two halves were separated immediately after heating. The two-dimensional temperature distribution induced in the central cross-section of the brain gel phantom through the center of balloon was recorded with a thermal imaging camera (Model PT1-170L-HT, Process Sensors Corporation, Germany).

2.5. Simulation of Balloon Implant Heating

Computer modeling of TBT balloon implant heating was performed in a human brain model to determine expected temperature distributions around the implant as a function of balloon diameter (d = 2, 3, 4 or 5 cm) and power (P) absorbed in the MNP solution from the magnetic field. Power was optimized to produce a minimum temperature of 40°C throughout a 5-mm annular shell of tumor bed tissue. Temperature simulations were computed using the bioheat equation (36) (equation 1) in a three-layer spherical model consisting of: a sphere representing the MNP solution with diameter d, a 5-mm annular shell surrounding the MNP domain corresponding to the tissue target, and a concentric sphere with a radius $r_{ext} = d + 5.5$ cm corresponding to the surrounding normal tissue. The bioheat equation is given by:

$$\rho c \frac{\partial T}{\partial t} = \nabla \cdot (k \nabla T) + \omega_b c_b (T_b - T) F(T) + Q_{met} \quad (1)$$

where t is time, T is temperature, T_b is arterial blood temperature (37°C), b index corresponds to blood, and the remaining properties are introduced in Table 1. To provide more realistic temperature estimations in the human brain, we accounted for the temperature-dependence of blood perfusion by introducing a scaling function $F(T)$ given by:

$$F(T) = \begin{cases} 1 + \alpha \exp\left(-\dfrac{(T - T_{cr})^2}{\beta}\right), & T \le T_{cr} \\ (1+\alpha)(1-\gamma) + \gamma\left[1 + \alpha \exp\left(-\dfrac{(T - T_{cr})^2}{\beta}\right)\right], & T > T_{cr} \end{cases} \quad (2)$$

with α, β and γ being curve-fitting parameters retrieved from experiments and T_{cr} the critical temperature at which perfusion starts to decrease due to thermal damage to the vasculature. Below T_{cr}, the scaling function presents a Gaussian profile that was first introduced by Tompkins et al. (37) and refined by Lang et al. (38) for muscle, fat, and tumor tissues. Based on the experimental measurements in large mammals by Lyons et al. (39) and Satoh et al. (40), we assume that the maximum blood perfusion occurs at 45°C (= T_{cr}) with a 2.5-fold increase above baseline ω_b, which results in α = 1.5. The parameter β is assumed to be the same as muscle: β = 12 (38). The perfusion behavior above T_{cr} has not been characterized for brain tissue. Thus, we developed a scaling function $F(T)$ for $T > T_{cr}$ assuming the same Gaussian profile, but with the equation recalibrated to enforce zero blood perfusion above 48°C (41), yielding γ = 3.1588.

For this proof of concept simulation, we used homogeneous white matter properties for the 5-mm target and surrounding tissue (Table 1). The MNP-mimicking heat source is embodied in an inward heat flux boundary condition given by $q_0 = \pi d^2 P/16$ (units of W/m^2), imposed at the implant surface at radius $r = d/2$. A convective heat flux was imposed at the external domain boundary (r_{ext}) with a convective coefficient of 200 W/m^2/K and a temperature of 37°C to account for surrounding convective losses due to blood flow and tissue perfusion (43). The simulations were performed in COMSOL Multiphysics v5.4 (Comsol Inc., Burlington MA). Finally to generate a mesh-independent solution, the mesh was refined so the maximum and minimum temperatures in the target did not change more than 0.002°C between mesh refinements. The resulting mesh parameters are shown in Table 2.

3. Results

Magnetic field measurements inside the head coil are shown in Figure 4 for 1.9 kW of applied power at 133 kHz. Note the large >10 cm diameter sweet spot near the coil center where the 5.2 kA/m field varies less than ± 10%. This level of field uniformity should produce nearly homogeneous power deposition in the 2-5 cm diameter MNP filled balloons regardless of location within the skull.

Figure 5A shows the reproducibility of power coupling into a MNP-filled test chamber with nine independent experiments using three different magnetic field strengths at 133 kHz. Note the nearly identical MNP heating rates obtained at each field strength during repeated trials. The two trials at 4.6 kA/m, five trials at 4.9 kA/m, and two trials at 5.3 kA/m are nearly indistinguishable on the plot, demonstrating the expected reproducibility of power absorption in magnetic nanoparticle fluid over both time and repeated field exposures.

As a more realistic test of heating capability, a GliaSite® balloon filled with 4.2 ml of MNP with 17 mg/ml Fe was inserted 4-cm deep in a life-size split-apart skull/brain tissue model

having thermal properties similar to zero perfusion white matter. After assembling the two halves of brain phantom in the center of the head coil and applying a 5 kA/m magnetic field at 133 kHz, temperature rise was highest at the balloon surface and fell off with increasing distance from the balloon as seen in Figure 6. After 30 min of heating, the temperature rise was 23°C at the balloon surface, 14°C at 5 mm, and 9°C at 10 mm radial distance from the balloon.

The uniformity of heating all around a MNP-filled balloon implant was assessed with a thermographic camera to capture the complete two dimensional heating pattern in the mid-depth cross-section of the split apart skull/brain phantom model. Figure 7A shows the geometry of the 2-cm diameter balloon centered in the life size head phantom. Figure 7B shows the thermal image obtained within 20 s after immersing the skull phantom in a 133 kHz magnetic field of 6.9 kA/m for 15 min followed by 6.2 kA/m for 5 min. As seen in Figure 7C, the balloon surface temperature rose 31°C above initial phantom temperature and fell off symmetrically in all directions. Temperatures throughout the 5-mm annular shell of “target tissue” rose at least 15°C or half the temperature rise of the balloon surface.

The computer simulations shown in Figure 8 demonstrate therapeutic 40 - 48.5°C heating of a 5-mm annular shell of tumor bed tissue (target) around 2-5 cm diameter TBT balloon implants in white matter with realistic temperature-dependent perfusion (Fig. 8A). Thermal conduction heating of tissue around the balloon implant is rapid and steady state is achieved in less than 20 min (Figure 8B). The required total absorbed power of 2.1 – 9.3 W for the different size balloons corresponds to 0.3-0.6 W/ml of nanoparticle solution, which generates the prescribed 40°C minimum temperature throughout the 5-mm tumor bed while maintaining the maximum below 48.5°C. Due to the rapid falloff of temperature radially beyond the tumor bed, a very beneficial localization of thermal dose occurs with minimal heating of surrounding normal brain. As quantified in the temperature-volume histogram of Figure 8D, 100% of the 5-mm rim target tissue is heated above the prescribed 40°C threshold for 2, 3, 4 or 5 cm diameter balloons, with only 8.7 - 16.5% (or 0.5 - 1.2 mm) of the target tissue exceeding 45°C. At the same time, 95% of all surrounding normal brain tissue remains below 38°C and is thus spared from significant thermal toxicity.

4. Discussion

There are over 1 million solid tumor resections per year in the United States which often leave positive margins after surgery. Of these, there are approximately 24,000 glioblastoma and 50,000 single brain metastases cases that are candidates for surgery (44, 45). It has been established that despite the infiltrative nature of glioblastomas, they recur within 2 cm of the original resection margins in over 90% of patients (46-49). Thus, the ability to deliver a more effective dose of radiation locally with less toxicity peripherally will help optimize treatment of this disease. Post-op therapy commonly includes radiation, however external beam treatment alone is unable to deliver sufficient dose to effectively treat tumor bed without complications in surrounding normal brain. Traditional multi-catheter brachytherapy seed implants and interstitial therapies produce non-uniform dose distributions with very high dose at the surface and much lower dose midway between sources. This is particularly so around the irregular shape resection cavities found in brain several months after surgery

and external beam radiation. Considering all, current therapeutic approaches involving extended fractionation EBRT followed sequentially by combination local boost therapies are expensive and an inconvenient use of remaining lifespan for the patient.

Combining hyperthermia with ionizing radiation enhances the radiation response in tumors by several mechanisms. Hyperthermia sensitizes tumor cells to radiation damage (50) and inhibits mechanisms that repair radiation damage (51). Hyperthermia stimulates blood flow and an associated increase in tissue oxygenation has been demonstrated in both animal (52, 53) and human tumors (54). Because much of the tumor mass has lower blood flow, lower extracellular pH, and is hypoxic and nutritionally deprived relative to surrounding normal tissue, tumor cells are more sensitive to hyperthermia (55, 56). Not only is oxygen a potent radiation sensitizer, the corresponding enhanced perfusion can significantly increase local delivery of chemotherapy (57) and tumor immunotherapeutic agents such as large antibodies (58). The complimentary effects of adjuvant hyperthermia are further enhanced since the cell cycle distribution of sensitivity to low LET radiation is the reverse of that of hyperthermia (59). Coincidentally, it has been shown in both transplantable animal tumors (60) and human melanoma (12, 13) that when hyperthermia and radiation are delivered simultaneously, the interaction between modalities, and therapeutic impact, are greater than if they are separated by time (61).

Previous clinical trials have investigated the addition of local heat to best available therapy of brain tumor volumes using either interstitial catheter-based microwave antennas (16) or ferromagnetic seeds (17, 62, 63), or multiple needle-injected magnetic nanoparticles (18, 19, 64). These studies all demonstrated substantial impact of adjuvant hyperthermia in spite of: a) imperfect catheter or injection track geometry relative to resection cavity shape, b) non-uniform heat delivery to resection cavity wall, c) non-uniform concentration of magnetic particles within the target tissue, and d) protracted timing of sequentially delivered therapies that were applied weeks apart and months after tumor resection. (16-19)It is well known that there are changes in the size and shape of a resection cavity in the months following surgery due to normal shifting of soft brain tissue as well as shrinkage and distortion of brain from EBRT. This transforms the treatment target from a simple annular rim of at-risk tissue around an approximately spherical cavity immediately after surgery to a convoluted irregular shape target. Moreover, the ~3 months required to complete post-surgical healing and fractionated radiotherapy provides critical time for tumor cells dislodged at the time of surgery to migrate deeper into surrounding normal brain. One impact of this post-surgical delay in treatment is a moving, expanding target for local therapy. New approaches are under investigation to distribute a sufficiently high concentration of magnetic nanoparticles throughout the region of brain tumor to generate appropriate temperature distributions (65, 66). One study investigated the inverse problem of calculating temperature within a solid tumor mass induced from a shell of magnetic particles entirely surrounding a spherical tumor (67). (68)Recent advances in the delivery of magnetic fluid hyperthermia were reviewed recently (69) including filling a natural body cavity with magnetic nanoparticle solution (68). Such approaches may be feasible when local toxicity of the nanoparticles and accumulation of magnetic material in the region are not an issue. For applications in brain tumor therapy, it is generally preferred to avoid leaving magnetic material in the brain that will complicate magnetic resonance follow up imaging.

As demonstrated in previous clinical trials that combined highly heterogeneous interstitial heat and brachytherapy dose distributions, HT offers a powerful boost to the RT anti-tumor effect without increasing normal tissue complications significantly. Even using interstitial implants delayed months after surgery, thermoradiotherapy clinical trials in primary GBM have (16)demonstrated a doubling of 2-year survival (16), (17)increased median survival from 13 to 24 months (17), and to 23.2 months (19). In retrospect, the difficulty in obtaining uniform dose coverage of all at-risk tissue with widely spaced ferroseeds, nanoparticles, or microwave antennas implanted into the irregular shape annular rim target around a resection cavity is easily appreciated. To improve upon the above thermoradiotherapy results, a new technology is required that can: 1) deliver heat and radiation doses more uniformly to at-risk tumor bed; 2) deliver both treatments simultaneously for maximum synergism; 3) be compatible with standard neurooncology procedures; and 4) be applied immediately after surgery before proliferation and spread of tumor cells into surrounding brain.

For this study, a magnetic induction heating system was constructed with 26 × 30 × 19 cm^3 head coil that accomplished the desired local heating of 2-cm diameter balloons filled with commercially available 17 mg/ml iron nanoparticles. It is well known that along with nanoparticle heating some amount of direct tissue heating results from induced eddy currents which are proportional to magnetic field-squared, frequency-squared, and radius-squared of eddy current path in tissue (70, 71). It is also well known that for a given size tissue load in a magnetic field, tissue will absorb energy from the field and heat at a similar rate when exposed to the same product of magnetic field and frequency (H × f) (72). Clinical studies by Maier-Hauff *et al.* (18, 19) have demonstrated that MNP-based heat treatments are safe and effective in humans using a 100 kHz magnetic field up to 13.5 kA/m together with iron oxide nanoparticles injected interstitially into brain, for an H × f product of 1.35 A/m·GHz.(18, 19) The maximum output of this system is 1.07 A/m·GHz as currently configured and only 0.8 A/m·GHz at the expected operating level. So the proposed TBT balloon heating approach offers improved patient safety due to reduced direct eddy current heating of brain relative to previous hyperthermia clinical trials that required higher field strengths to activate a smaller volume of dispersed magnetic material. Using a moderate 5.7 kA/m field at 133 kHz (~45% lower H × f product than that used by Maier-Hauff *et al.*(19) which should lead to ~70% lower direct tissue heating), the system produced the required 0.5 W/ml within a 2-cm diameter nanoparticle-filled balloon anywhere inside the head coil including the broad minimum field “sweet spot” in coil center (Figure 4). Though this field is sufficient to heat human brain around any of the proposed 2-5 cm diameter balloons, higher fields are easily achieved safely if necessary and the system was tested for over 60 minutes continuous operation at 8.1 kA/m i(19)n the coil center, which produced 0.85 W/ml in the 2-cm diameter balloon. In subsequent application to heating resection cavities in larger diameter tissue regions such as human abdomen or pelvis, additional strategies may be useful to further enhance local nanoparticle heating such as power modulation of the magnetic field (73-75). Our experimental results with magnetic nanoparticles show excellent repeatability of heating, even when reusing the same nanoparticle solution and silicone balloon catheter >30 times over 5 months. These experiments clearly demonstrate that commercially available nanoparticles can be used to produce therapeutic temperatures (e.g. 40-48°C) all around implanted balloon catheters such as the GliaSite® and presumably the

similarly constructed double wall balloon of Fig. 1. Moreover the experiments demonstrate repeatability of heating characteristics after storing the MNP-filled balloon in a refrigerator for long periods between trials.

Since the experimental phantom studies do not include critically important blood perfusion, we conducted computational simulations to investigate the feasibility of heating perfused human tissue. Although the simulated geometry is straightforward (concentric spheres), the temperature-dependent parameter $F(T)$ of Eqn. 2 transforms the bioheat equation into a non-linear partial differential equation so that available analytical solutions (e.g. developed by Rodrigues et al. (43) or Andra et al. (66)), are not applicable. Thus, we performed numerical simulations using commercially available software with a temperature-dependent blood perfusion function that includes three white matter-specific parameters: ω_b, T_{cr}, and a. Additionally, a β parameter derived from muscle properties and γ were introduced in this study for $T > T_{cr} = 45$°C to guarantee zero blood perfusion above 48°C. Both the threshold of 48°C and the Gaussian profile between 45-48°C are assumptions based on experimental work performed in mice (41). The impact of this uncertainly above 45°C is limited for two reasons: (1) the tissue volume above 45°C is only about 1-mm in thickness immediately adjacent to the balloon (Fig. 8C); and (2) we expect a thin coating (likely of the order of 1 mm) of blood and/or cerebrospinal fluid surrounding the balloon to have no perfusion and thus can exceed 45°C without harm. Furthermore, we modeled healthy brain tissue throughout the 5-mm annular shell target, though we might anticipate somewhat impaired blood perfusion due to the surgical resection. Thus, modeling healthy perfusion throughout the 5-mm tumor bed should be a worst-case scenario, such that we might use balloon surface temperatures somewhat lower than our simulations or expect to penetrate somewhat deeper than 5-mm with our 40°C goal. Despite the simplicity of the anatomical model to date, these simulations indicate that it is feasible to heat well-perfused brain using the MNP balloon approach. Future numerical studies will accommodate more precise anatomical models that include the presence of large vessels, CSF, and the transient behavior of blood perfusion (e.g., (75)).

The expected outcome of using the proposed thermobrachytherapy balloon implant is the first ever clinically practical device capable of delivering simultaneous and uniform HT and RT to resection cavity wall targets. This device should produce minimal normal tissue damage >10-mm from the resection margin and significantly reduce the time (≤1 week) and cost of thermobrachytherapy. The technique is compatible with existing surgical, radiation and chemotherapy procedures. Although this approach will require lower magnetic field strength to heat the nanoparticle filled balloon than previous clinical trials, contraindications to using this approach will include the presence of large metallic objects in the head, similar to previous clinical investigations of magnetic field heating inside the head (19, 62, 64, 76-79). By adapting proven technologies like silicone balloon brain implants (8, 80) and inflatable catheter-based HDR brachytherapy (9, 10) in combination with proven heating approaches like magnetic field induced heating of ferromagnetic seeds (71, 77, 79, 81) and magnetic nanoparticles (18, 19, 82), this approach should see expedited clinical implementation due to successful clinical precedent and established regulatory pathway for all component technologies.

It has been 22 years since a randomized clinical trial showed a statistically significant doubling of 2-year survival over the best available combination treatment for GBM. Among other challenges that limited the impact of that trial, the protocol required a delay of 3.5 months before sequential delivery of local HT and RT treatments to the tumor bed via a small number of interstitial implant catheters. It has been 30 years since pre-clinical data demonstrated a dramatic enhancement of local RT effect without accompanying increase in long term toxicity by combining heat and radiation simultaneously (13). The ensuing decades have seen no advances in commercial equipment to deliver uniform heat and radiation to a resection cavity tumor bed and no significant improvement in survival or quality of life for the general population of GBM patients. A system that can provide combination HT and RT simultaneously for maximum TER and uniformly distributed to cancer cells all around the resection cavity is long overdue. The early prototype system first described in a conference proceedings article (83) and tested in this feasibility study addresses this dire need for new equipment and offers the additional benefit that all thermoradiotherapy can be completed within 1 week of surgery, before tumor cell proliferation and expansion deeper into surrounding brain.

One issue that has been considered carefully in this development regards the ability to conform a primarily spherical shape balloon into intimate contact with the resection cavity wall for good thermal conduction out into surrounding brain. The FDA-approved GliaSite balloon (84, 85), used successfully in over 500 brain tumor patients, provides excellent precedent for the proposed thermobrachytherapy balloon. The GliaSite provided a straight-forward protocol for determining the balloon fill volume as well as the radiation dosing scheme required to achieve the intended depth of penetration (86). At the time of tumor resection, the balloon was filled with an observed volume of saline to gently displace the margins of the resection cavity into a spherical shape. With experience, this was easily achieved with little to no risk of creating untoward mass effect in surrounding brain. The saline was subsequently withdrawn and the same volume of radioactive liquid used to refill the balloon for the multi-day radiation treatment. Our proposed procedure will replace the radiation fluid with a magnetic nanoparticle solution for heating and a retractable HDR brachytherapy source inserted to the center of balloon. This configuration maximizes uniformity of radiation and heat delivered to the resection cavity wall with consequent spherically symmetric dose distribution to surrounding brain (86). A good illustration of the preferred spherically symmetric dosimetry in brain around a GliaSite balloon implant is shown in Chan et al. (84). Heating of the brain will be monitored via a temperature probe inside the thermobrachytherapy balloon and the temperature gradient falloff into surrounding tissue determined via treatment planning. As with other hyperthermia treatments, tissue temperature immediately adjacent to large heat sinks like CSF spaces and large vascularity will not be known exactly. However, past experience of our group with GliaSite balloons, interstitial laser and microwave antenna heat sources have shown that source placement can help accommodate expected temperature heterogeneities while some temperature variation within the treatment volume is unavoidable.

Although this research paves the way for fast well-focused therapy of at-risk tissue around a surgical resection cavity, future clinical trials must establish whether local therapy for GBM is sufficient to eliminate viable tumor cells in the resection cavity margin when treatment is

completed immediately after surgery or if there remains a need to add external beam RT, systemic chemotherapy, and/or immune boost therapies. The proposed 46-48°C balloon surface temperatures simulated in this work are a proposed starting point for clinical investigations; higher temperatures are easily obtained if determined useful clinically. The current team of neurooncologists involved in this project believe that in a majority of patients, GBMs recur close to the original surgical cavity and not several cm distant in brain. Thus a 48°C surface temperature treating 5-8 mm rim of tissue (depending on surrounding perfusion) should be a good starting point for clinical studies that might push higher in temperature when tolerable clinically. The endpoint is overall patient satisfaction, which includes not only duration of response, but also time of therapy and quality of life (QOL) over the duration of response. The proposed approach anticipates improved QOL from: a) giving critical time back to the patient by completing all therapy in 1 week, b) improving the localization of HT and RT in tumor bed which should reduce normal brain toxicity, and c) reducing or eliminating EBRT which should further reduce neurocognitive deficit throughout a much longer anticipated survival period.

5. Conclusions

We describe a dual-modality thermobrachytherapy (TBT) balloon temporary implant device for treating at-risk tissue around a GBM tumor resection cavity with HDR brachytherapy and simultaneous local heat via external magnetic field activated nanoparticles. Temperature simulations of heating in well-perfused white matter demonstrate the ability to heat a 5-mm annular rim of tumor bed in brain to a therapeutic 40 - 48°C by absorbing <0.5 W/ml in 2-5 cm diameter nanoparticle-filled balloons. Laboratory measurements repeated over a 5-month timeframe demonstrate the ability to reproducibly deposit over 3 times the required power density in a 2-cm diameter balloon filled with commercially available GMP-manufactured magnetic nanoparticles (17 mg/ml iron) activated with a magnetic field of 5.7 kA/m at 133 kHz. This field is well below the level that has proven safe in previous human clinical trials. The proposed TBT balloon implant has the potential to simultaneously deliver radiation and heat more uniformly to tumor bed than alternative interstitial implant technologies and to generate a thermal enhancement ratio up to 5.0 for significantly enhanced therapeutic effect compared to RT treatment alone. The well-localized conformal dosimetry obtained with this new device should provide improved patient outcomes with lower complications in surrounding healthy brain. The reduced overall time of therapy applied immediately after surgery should help improve quality of life as well as survival for patients with glioblastoma multiforme.

Supplementary Material

Refer to Web version on PubMed Central for supplementary material.

Acknowledgments

The authors would like to acknowledge support from NIH R41 CA-239815, Heather Rose and the Thomas Jefferson Innovation Pillar, the Department of Radiation Oncology, and collaborators Robert and Ricardo Ruffini of AMF Life Systems, Auburn Hills, MI who provided the induction heating system and head coil used in the experimental measurements. The authors also acknowledge helpful guidance from Janet Kwiatkowski at MAE Group, and graphical assistance from Daniel Whitzer and Anthony Sorendino.

Funding

Research reported in this publication was supported by the National Cancer Institute of the National Institutes of Health under Award Number R41CA239815. The content is solely the responsibility of the authors and does not necessarily represent the official views of the National Institutes of Health.

References

1. Weller M, Le Rhun E, Preusser M, Tonn JC, Roth P. How we treat glioblastoma. ESMO Open. 2019;4(Suppl 2):e000520. [PubMed: 31297242]
2. Johnson DR, O'Neill BP. Glioblastoma survival in the United States before and during the temozolomide era. J Neurooncol. 2012;107(2):359–64. [PubMed: 22045118]
3. Delgado-López PD, Corrales-García EM. Survival in glioblastoma: a review on the impact of treatment modalities. Clinical and Translational Oncology. 2016;18(11):1062–71. [PubMed: 26960561]
4. Chinot OL, de La Motte Rouge T, Moore N, Zeaiter A, Das A, Phillips H, et al. AVAglio: Phase 3 trial of bevacizumab plus temozolomide and radiotherapy in newly diagnosed glioblastoma multiforme. Adv Ther. 2011;28(4):334–40. [PubMed: 21432029]
5. Gilbert MR, Dignam JJ, Armstrong TS, Wefel JS, Blumenthal DT, Vogelbaum MA, et al. A randomized trial of bevacizumab for newly diagnosed glioblastoma. N Engl J Med. 2014;370(8):699–708. [PubMed: 24552317]
6. Stupp R, Hegi ME, Mason WP, van den Bent MJ, Taphoorn MJ, Janzer RC, et al. Effects of radiotherapy with concomitant and adjuvant temozolomide versus radiotherapy alone on survival in glioblastoma in a randomised phase III study: 5-year analysis of the EORTC-NCIC trial. Lancet Oncol. 2009;10(5):459–66. [PubMed: 19269895]
7. Hegi ME, Diserens AC, Gorlia T, Hamou MF, de Tribolet N, Weller M, et al. MGMT gene silencing and benefit from temozolomide in glioblastoma. N Engl J Med. 2005;352(10):997–1003. [PubMed: 15758010]
8. Rogers LR, Rock JP, Sills AK, Vogelbaum MA, Suh JH, Ellis TL, et al. Results of a phase II trial of the GliaSite radiation therapy system for the treatment of newly diagnosed, resected single brain metastases. J Neurosurg. 2006;105(3):375–84. [PubMed: 16961129]
9. Njeh CF, Saunders MW, Langton CM. Accelerated partial breast irradiation (APBI): A review of available techniques. Radiat Oncol. 2010;5:90. [PubMed: 20920346]
10. Selvaraj RN, Bhatnagar A, Beriwal S, Huq MS, Heron DE, Sonnik D, et al. Breast skin doses from brachytherapy using MammoSite HDR, intensity modulated radiation therapy, and tangential fields techniques. Technol Cancer Res Treat. 2007;6(1):17–22.
11. Dewey WC. Arrhenius relationships from the molecule and cell to the clinic. Int J Hyperthermia. 2009;25(1):3–20. [PubMed: 19219695]
12. Overgaard J. Simultaneous and sequential hyperthermia and radiation treatment of an experimental tumor and its surrounding normal tissue in vivo. Int J Radiat Oncol Biol Phys. 1980;6(11):1507–17. [PubMed: 7462053]
13. Overgaard J. The current and potential role of hyperthermia in radiotherapy. Int J Radiat Oncol. 1989;16:535–49.
14. Datta NR, Ordonez SG, Gaipl US, Paulides MM, Crezee H, Gellermann J, et al. Local hyperthermia combined with radiotherapy and-/or chemotherapy: recent advances and promises for the future. Cancer Treatment Reviews. 2015;41(9):742–53. [PubMed: 26051911]
15. Hurwitz MD, Stauffer PR. Hyperthermia, radiation and chemotherapy: the role of heat in multidisciplinary cancer care. Semin Oncol. 2014;41(6):714–29. [PubMed: 25499632]
16. Sneed PK, Stauffer PR, McDermott MW, Diederich CJ, Lamborn KR, Prados MD, et al. Survival benefit of hyperthermia in a prospective randomized trial of brachytherapy boost +/− hyperthermia for glioblastoma multiforme. International Journal of Radiation Oncology, Biology and Physics. 1998;40(2):287–95.
17. Stea B, Rossman K, Kittelson J, Shetter A, Hamilton A, Cassady JR. Interstitial irradiation versus interstitial thermoradiotherapy for supratentorial malignant gliomas: a comparative survival analysis. Int J Radiat Oncol Biol Phys. 1994;30(3):591–600. [PubMed: 7928490]

18. Maier-Hauff K, Rothe R, Scholz R, Gneveckow U, Wust P, Thiesen B, et al. Intracranial thermotherapy using magnetic nanoparticles combined with external beam radiotherapy: results of a feasibility study on patients with glioblastoma multiforme. Journal of Neuro-Oncology. 2007;81(1):53–60. [PubMed: 16773216]
19. Maier-Hauff K, Ulrich F, Nestler D, Niehoff H, Wust P, Thiesen B, et al. Efficacy and safety of intratumoral thermotherapy using magnetic iron-oxide nanoparticles combined with external beam radiotherapy on patients with recurrent glioblastoma multiforme. J Neurooncol. 2011;103(2):317–24. [PubMed: 20845061]
20. Strobel H, Baisch T, Fitzel R, Schilberg K, Siegelin MD, Karpel-Massler G, et al. Temozolomide and Other Alkylating Agents in Glioblastoma Therapy. Biomedicines. 2019;7(3):69.
21. Shah JL, Li G, Shaffer JL, Azoulay MI, Gibbs IC, Nagpal S, et al. Stereotactic Radiosurgery and Hypofractionated Radiotherapy for Glioblastoma. Neurosurgery. 2018;82(1):24–34. [PubMed: 28605463]
22. Sneed PK, Lamborn KR, Larson DA, Prados MD, Malec MK, McDermott MW, et al. Demonstration of brachytherapy boost dose-response relationships in glioblastoma multiforme. International Journal of Radiation Oncology, Biology, Physics. 1996;35(1):37–44.
23. Kickingereder P, Hamisch C, Suchorska B, Galldiks N, Visser-Vandewalle V, Goldbrunner R, et al. Low-dose rate stereotactic iodine-125 brachytherapy for the treatment of inoperable primary and recurrent glioblastoma: single-center experience with 201 cases. J Neurooncol. 2014;120(3):615–23. [PubMed: 25151509]
24. Gessler DJ, Ferreira C, Dusenbery K, Chen CC. GammaTile(®): Surgically targeted radiation therapy for glioblastomas. Future Oncol. 2020.
25. Xing WK, Shao C, Qi ZY, Yang C, Wang Z. The role of Gliadel wafers in the treatment of newly diagnosed GBM: a meta-analysis. Drug Des Devel Ther. 2015;9:3341–8.
26. Ashby LS, Smith KA, Stea B. Gliadel wafer implantation combined with standard radiotherapy and concurrent followed by adjuvant temozolomide for treatment of newly diagnosed high-grade glioma: a systematic literature review. World journal of surgical oncology. 2016;14(1).
27. Mahaley MS Jr. Neuro-oncology index and review (adult primary brain tumors). Radiotherapy, chemotherapy, immunotherapy, photodynamic therapy. Journal of Neuro-Oncology. 1991;11:85–147. [PubMed: 1744686]
28. Tivnan A, Heilinger T, Lavelle EC, Prehn JHM. Advances in immunotherapy for the treatment of glioblastoma. Journal of Neuro-Oncology. 2017;131(1):1–9. [PubMed: 27743144]
29. Kim Y. Dosimetric impact of source-positioning uncertainty in high-dose-rate balloon brachytherapy of breast cancer. Journal of Contemporary Brachytherapy. 2015;5:387–96.
30. Monroe JI, Dempsey JF, Dorton JA, Mutic S, Stubbs JB, Markman J, et al. Experimental validation of dose calculation algorithms for the GliaSite RTS, a novel 125I liquid-filled balloon brachytherapy applicator. Med Phys. 2001;28(1):73–85. [PubMed: 11213925]
31. Cai X, Zhu Q, Zeng Y, Zeng Q, Chen X, Zhan Y. Manganese Oxide Nanoparticles As MRI Contrast Agents In Tumor Multimodal Imaging And Therapy. International Journal of Nanomedicine. 2019;Volume 14:8321–44. [PubMed: 31695370]
32. Wu K, Su D, Liu J, Saha R, Wang J-P. Magnetic nanoparticles in nanomedicine: a review of recent advances. Nanotechnology. 2019;30(50):502003. [PubMed: 31491782]
33. Ivkov R. Magnetic nanoparticle hyperthermia: a new frontier in biology and medicine? Int J Hyperthermia. 2013;29(8):703–5. [PubMed: 24219798]
34. Mahmoudi K, Bouras A, Bozec D, Ivkov R, Hadjipanayis C. Magnetic hyperthermia therapy for the treatment of glioblastoma: a review of the therapy's history, efficacy and application in humans. Int J Hyperthermia. 2018;34(8):1316–28. [PubMed: 29353516]
35. Goldstein R, inventor; AMF Lifesystems, LLC, assignee. Induction coil for low radiofrequency applications in a human head USA patent US 10,286,223 B2. 2019 5 14, 2019.
36. Pennes HH. Analysis of tissue and arterial blood temperatures in the resting human forearm. Journal of Applied Physiology. 1948;1:93–122. [PubMed: 18887578]
37. Tompkins DT, Vanderby R, Klein SA, Beckman WA, Steeves RA, Frye DM, et al. Temperature-dependent versus constant-rate blood perfusion modelling in ferromagnetic thermoseed

hyperthermia: results with a model of the human prostate. Int J Hyperthermia. 1994;10(4):517–36. [PubMed: 7963808]

38. Lang J, Erdmann B, Seebass M. Impact of nonlinear heat transfer on temperature control in regional hyperthermia. IEEE Trans Biomed Eng. 1999;46(9):1129–38. [PubMed: 10493076]
39. Lyons BE, Samulski TV, Cox RS, Fessenden P. Heat loss and blood flow during hyperthermia in normal canine brain. I: Empirical study and analysis. Int J Hyperthermia. 1989;5(2):225–47. [PubMed: 2926187]
40. Satoh T, Nakasone S, Nishimoto A. Cerebral blood flow response to the tissue temperature in tumour and brain tissues. Int J Hyperther. 1989;5:683–96.
41. Song CW, Park HJ, Lee CK, Griffin R. Implications of increased tumor blood flow and oxygenation caused by mild temperature hyperthermia in tumor treatment. Int J Hyperthermia. 2005;21(8):761–7. [PubMed: 16338859]
42. Hasgall P, Di Gennaro F, Baumgartner C, Neufeld E, Lloyd B, Gosselin M, et al. ITIS database for thermal and electromagnetic parameters of biological tissues (Version 4.0). itis.swiss/database, 2018.
43. Rodrigues D, Pereira J, Limão-Vieira P, Stauffer P, Maccarini P. Study of the one dimensional and transient bioheat transfer equation: multilayer solution development and applications. International Journal of Heat and Mass Transfer. 2013;62(1):153–62. [PubMed: 24511152]
44. Ostrom QT, Gittleman H, Xu J, Kromer C, Wolinsky Y, Kruchko C, et al. CBTRUS Statistical Report: Primary Brain and Other Central Nervous System Tumors Diagnosed in the United States in 2009-2013. Neuro Oncol. 2016;18(suppl_5):v1–v75. [PubMed: 28475809]
45. Sperduto PW, Chao ST, Sneed PK, Luo X, Suh J, Roberge D, et al. Diagnosis-specific prognostic factors, indexes, and treatment outcomes for patients with newly diagnosed brain metastases: a multi-institutional analysis of 4,259 patients. Int J Radiat Oncol Biol Phys. 2010;77(3):655–61. [PubMed: 19942357]
46. Hochberg FH, Pruitt A. Assumptions in the radiotherapy of glioblastoma. Neurology. 1980;30(9):907–11. [PubMed: 6252514]
47. Liang BC, Thornton AF Jr., Sandler HM, Greenberg HS. Malignant astrocytomas: focal tumor recurrence after focal external beam radiation therapy. Journal of Neurosurgery. 1991;75:559–63. [PubMed: 1653309]
48. Proescholdt MA, Macher C, Woertgen C, Brawanski A. Level of evidence in the literature concerning brain tumor resection. Clin Neurol Neurosurg. 2005;107(2):95–8. [PubMed: 15708222]
49. Stummer W, van den Bent MJ, Westphal M. Cytoreductive surgery of glioblastoma as the key to successful adjuvant therapies: new arguments in an old discussion. Acta Neurochir (Wien). 2011;153(6):1211–8. [PubMed: 21479583]
50. Raaphorst GP, Feeley MM, Danjoux CE, DaSilva V, Gerig LH. Hyperthermia enhancement of radiation response and inhibition of recovery from radiation damage in human glioma cells. Int J Hyperther. 1991;7:629–41.
51. Genet SC, Fujii Y, Maeda J, Kaneko M, Genet MD, Miyagawa K, et al. Hyperthermia inhibits homologous recombination repair and sensitizes cells to ionizing radiation in a time- and temperature-dependent manner. J Cell Physiol. 2013;228(7):1473–81. [PubMed: 23254360]
52. Song CW. Effect of local hyperthermia on blood flow and microenvironment: A review. Cancer Research (Supplement). 1984;44:4721–30.
53. Song CW, Park H, Griffin RJ. Improvement of tumor oxygenation by mild hyperthermia. Radiat Res. 2001;155(4):515–28. [PubMed: 11260653]
54. Brizel DM, Scully SP, Harrelson JM, Layfield LJ, Dodge RK, Charles HC, et al. Radiation therapy and hyperthermia improve the oxygenation of human soft tissue sarcomas. Cancer Res. 1996;56(23):5347–50. [PubMed: 8968082]
55. Gillette EL, Ensley BA. Effect of heat, radiation and pH on mouse mammary tumor cells. Int J Radiat Oncol Biol Phys. 1983;9(10):1521–5. [PubMed: 6629892]
56. Herman TS, Teicher BA, Holden SA, Collins LS. Interaction of hyperthermia and radiation in murine cells: hypoxia and acidosis in vitro, tumor subpopulations in vivo. Cancer Res. 1989;49(12):3338–43. [PubMed: 2720686]

57. Ware MJ, Krzykawska-Serda M, Chak-Shing Ho J, Newton J, Suki S, Law J, et al. Optimizing non-invasive radiofrequency hyperthermia treatment for improving drug delivery in 4T1 mouse breast cancer model. Sci Rep. 2017;7:43961. [PubMed: 28287120]
58. Centelles MN, Wright M, Gedroyc W, Thanou M. Focused ultrasound induced hyperthermia accelerates and increases the uptake of anti-HER-2 antibodies in a xenograft model. Pharmacol Res. 2016;114:144–51. [PubMed: 27771465]
59. Westra A, Dewey WC. Variation in sensitivity to heat shock during the cell cycle of Chinese hamster cells in vitro. International Journal of Radiation Biology. 1971;19:467–77.
60. Gillette EL, Ensley BA. Effect of heating order on radiation response of mouse tumor and skin. Int J Radiat Oncol Biol Phys. 1979;5(2):209–13. [PubMed: 110735]
61. Overgaard J, Overgaard M. Hyperthermia as an adjuvant to radiotherapy in the treatment of malignant melanoma. Int J Hyperther. 1987;3:483–501.
62. Stea B, Cetas TC, Cassady JR, Guthkelch AN, Iacono R, Lulu B, et al. Interstitial thermoradiotherapy of brain tumors: preliminary results of a phase I clinical trial. Int J Radiat Oncol. 1990;19:1463–71.
63. Stea B, Rossman K, Kittelson J, Lulu B, Shetter A, Cassady JR, et al. A comparison of survival between radiosurgery and stereotactic implants for malignant astrocytomas. Acta Neurochir Suppl. 1994;62:47–54. [PubMed: 7717135]
64. Thiesen B, Jordan A. Clinical applications of magnetic nanoparticles for hyperthermia. Int J Hyperther. 2008;24(6):467–74.
65. Bellizzi G, Bucci OM, Chirico G. Numerical assessment of a criterion for the optimal choice of the operative conditions in magnetic nanoparticle hyperthermia on a realistic model of the human head. Int J Hyperthermia. 2016;32(6):688–703. [PubMed: 27268850]
66. Andra W, d'Ambly C, Hergt R, Hilger I, Kaiser W. Temperature distribution as function of time around a smallspherical heat source of local magnetic hyperthermia Journal of Magnetism and Magnetic Materials. 1999;194:197–203.
67. Giordano MA, Gutierrez G, Rinaldi C. Fundamental solutions to the bioheat equation and their application to magnetic fluid hyperthermia. Int J Hyperther. 2010;26(5):475–84.
68. Oliveira TR, Stauffer PR, Lee CT, Landon CD, Etienne W, Ashcraft KA, et al. Magnetic fluid hyperthermia for bladder cancer: a preclinical dosimetry study. Int J Hyperthermia. 2013;29(8):835–44. [PubMed: 24050253]
69. Das P, Colombo M, Prosperi D. Recent advances in magnetic fluid hyperthermia for cancer therapy. Colloids and surfaces B, Biointerfaces. 2019;174:42–55. [PubMed: 30428431]
70. Stauffer PR, Cetas TC, Jones RC. Magnetic induction heating of ferromagnetic implants for inducing localized hyperthermia in deep-seated tumors. IEEE Trans Biomed Eng. 1984;31(2):235–51. [PubMed: 6706353]
71. Stauffer PR, Cetas TC, Fletcher AM, DeYoung DW, Dewhirst MW, Oleson JR, et al. Observations on the use of ferromagnetic implants for inducing hyperthermia. IEEE Trans Biomed Eng. 1984;31(1):76–90. [PubMed: 6724613]
72. Atkinson WJ, Brezovich IA, Chakraborty DP. Usable frequencies in hyperthermia with thermal seeds. IEEE Trans Biomed Eng. 1984;31(1):70–5. [PubMed: 6724612]
73. Attaluri A, Kandala SK, Wabler M, Zhou H, Cornejo C, Armour M, et al. Magnetic nanoparticle hyperthermia enhances radiation therapy: A study in mouse models of human prostate cancer. Int J Hyperthermia. 2015;31(4):359–74. [PubMed: 25811736]
74. Ivkov R, DeNardo SJ, Daum W, Foreman AR, Goldstein RC, Nemkov VS, et al. Application of high amplitude alternating magnetic fields for heat induction of nanoparticles localized in cancer. Clin Cancer Res. 2005;11(19 Pt 2):7093s–103s. [PubMed: 16203808]
75. Kandala SK, Liapi E, Whitcomb LL, Attaluri A, Ivkov R. Temperature-controlled power modulation compensates for heterogeneous nanoparticle distributions: a computational optimization analysis for magnetic hyperthermia. Int J Hyperther. 2019;36(1):115–29.
76. Jordan A, Wust P, Fahling H, John W, Hinz A, Felix R. Inductive heating of ferrimagnetic particles and magnetic fluids: physical evaluation of their potential for hyperthermia. 1993. Int J Hyperthermia. 2009;25(7):499–511. [PubMed: 19848612]

77. Stauffer P, Vasilchenko I, Osintsev A, Rodrigues D, Bar-Ad V, Hurwitz M, et al. Tumor bed brachytherapy for locally advanced laryngeal cancer: a feasibility assessment of combination with ferromagnetic hyperthermia. Biomedical Physics & Engineering Express. 2016;2:1–12.

78. Vasil'chenko IL, Vinogradov VM, Pastushenko DA, Osintsev AM, Maitakov AL, Rynk VV, et al. Use of local induced hyperthermia in the treatment of malignant tumors. Vopr Onkol. 2013;59(2):84–9. [PubMed: 23814855]

79. Mack CF, Stea B, Kittelson JM, Shimm DS, Sneed PK, Phillips TL, et al. Interstitial thermoradiotherapy with ferromagnetic implants for locally advanced and recurrent neoplasms. Int J Radiat Oncol. 1993;27:109–15.

80. Gabayan AJ, Green SB, Sanan A, Jenrette J, Schultz C, Papagikos M, et al. GliaSite brachytherapy for treatment of recurrent malignant gliomas: a retrospective multi-institutional analysis. Neurosurgery. 2006;58(4):701–9. [PubMed: 16575334]

81. Stea B, Kittelson J, Cassady JR, Hamilton A, Guthkelch N, Lulu B, et al. Treatment of malignant gliomas with interstitial irradiation and hyperthermia. Int J Radiat Oncol Biol Phys. 1992;24(4):657–67. [PubMed: 1429088]

82. Jordan A, Maier-Hauff K. Magnetic nanoparticles for intracranial thermotherapy. Journal of Nanoscience & Nanotechnology. 2007;7(12):4604–6. [PubMed: 18283851]

83. Stauffer P, Rodrigues D, Goldstein R, Nguyen T, Doyle L, Bar-Ad V, et al., editors. Dual Modality Implant for Simultaneous Magnetic Nanoparticle Heating and Brachytherapy Treatment of Tumor Resection Cavities in Brain IEEE/MTT-S International Microwave Syposium Proceedings; 2018; Philadelphia: Institute of Electrical and Electronics Engineers.

84. Chan TA, Weingart JD, Parisi M, Hughes MA, Olivi A, Borzillary S, et al. Treatment of recurrent glioblastoma multiforme with GliaSite brachytherapy. Int J Radiat Oncol Biol Phys. 2005;62(4):1133–9. [PubMed: 15990019]

85. Welsh J, Sanan A, Gabayan AJ, Green SB, Lustig R, Burri S, et al. GliaSite brachytherapy boost as part of initial treatment of glioblastoma multiforme: a retrospective multi-institutional pilot study. Int J Radiat Oncol Biol Phys. 2007;68(1):159–65. [PubMed: 17331666]

86. Dempsey JF, Williams JA, Stubbs JB, Patrick TJ, Williamson JF. Dosimetric properties of a novel brachytherapy balloon applicator for the treatment of malignant brain-tumor resection-cavity margins. Int J Radiat Oncol Biol Phys. 1998;42(2):421–9. [PubMed: 9788425]

87. Stauffer P, Bar-Ad V, Hurwitz M, Luginbuhl A, Marcolongo M, Rodrigues D, et al., inventors USPTO 16/086,733 Tumor Bed Implant for Multimodality Treatment of At Risk Tissue Surrounding a Resection Cavity. 2019 3-31-17.

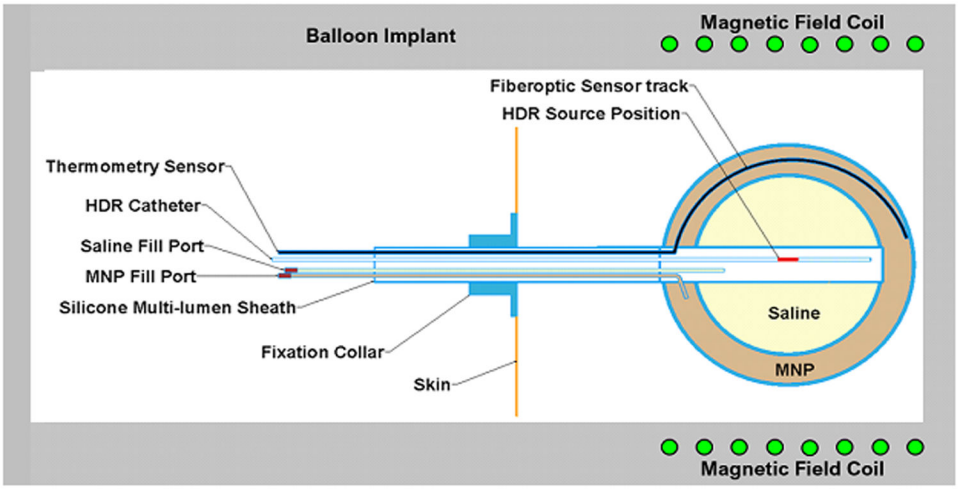

Figure 1.

Thermobrachytherapy balloon design. The outer balloon is filled with MNP to heat tumor bed and the inner balloon is inflated with saline to expand the resection cavity wall into more advantageous near-spherical geometry. A catheter extends through the flexible shaft and along the outer balloon wall to insert a temperature monitoring and control sensor. A central catheter extends from the surface to the balloon center for inserting an HDR radiation source. Two catheters extend from valved ports to fill the balloons with saline and MNP solution.

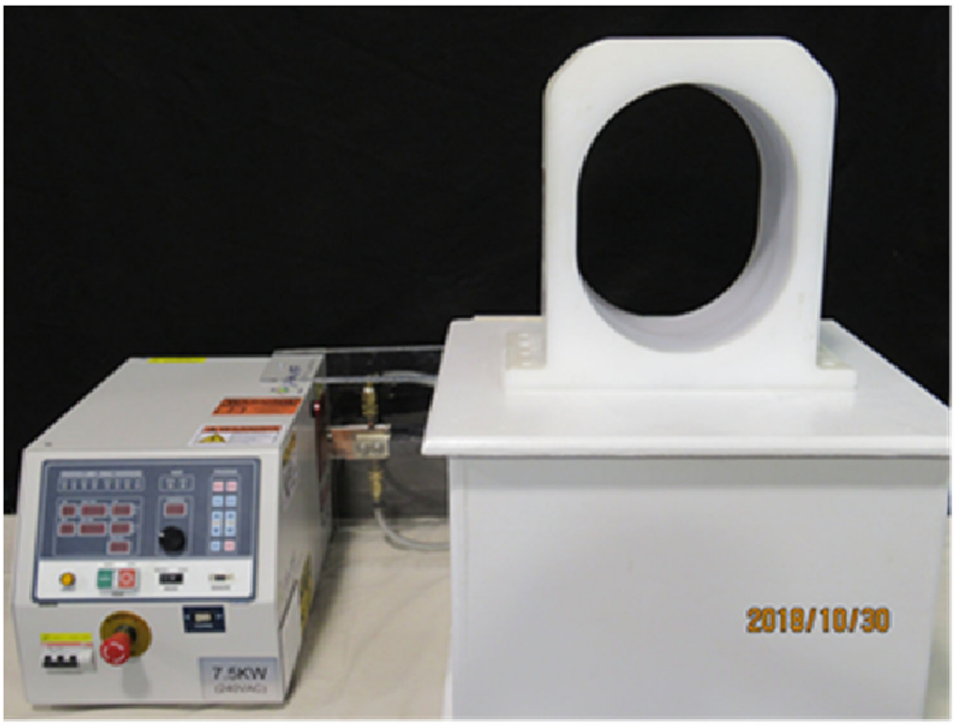

Figure 2.

Photograph of laboratory induction heating system used for initial characterization of heating from MNP-filled balloon implants, including radiofrequency power amplifier, matching network and water-cooled 26 × 31 × 20 cm^3 head coil (AMF Life Systems, Auburn Hills MI).

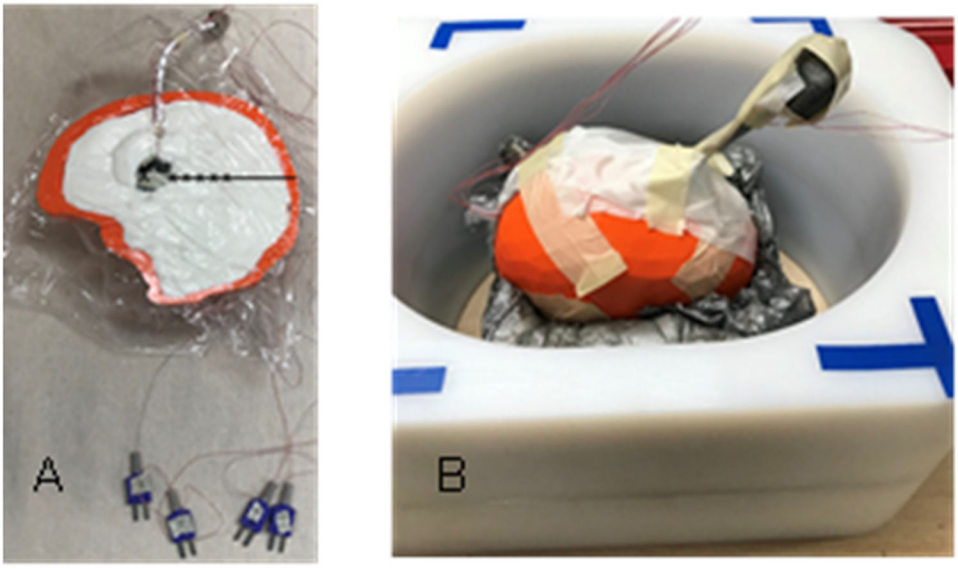

Figure 3.

Experimental setup of magnetic nanoparticle (MNP) balloon implant heating: (A) 2-cm diameter MNP-filled balloon buried 4-cm deep in the central plane of a split-apart human skull model that is filled with brain tissue-equivalent phantom and 2.5-mm spaced thermocouples to measure radial penetration of heating. (B) Split-apart skull/brain model assembled inside the head coil for application of radiofrequency magnetic field.

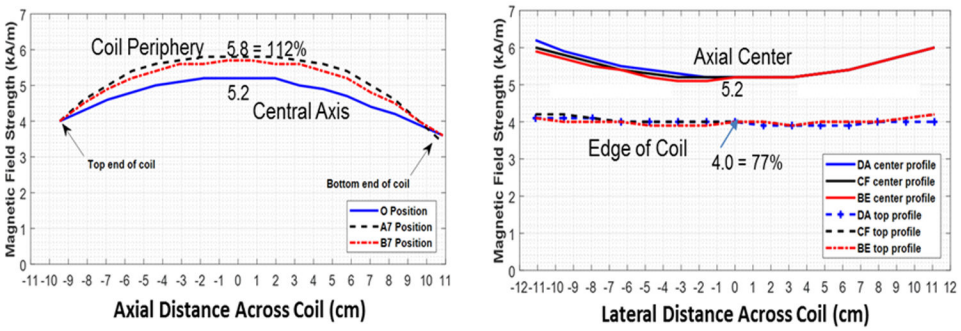

Figure 4.

Magnetic field profiles in head coil. (A) Magnetic field as a function of position along the coil axis in the center (blue) and two positions along the outer casing of coil. (B) Magnetic field profiles horizontally and vertically across the coil at coil center (solid) and at each end of coil (dash).

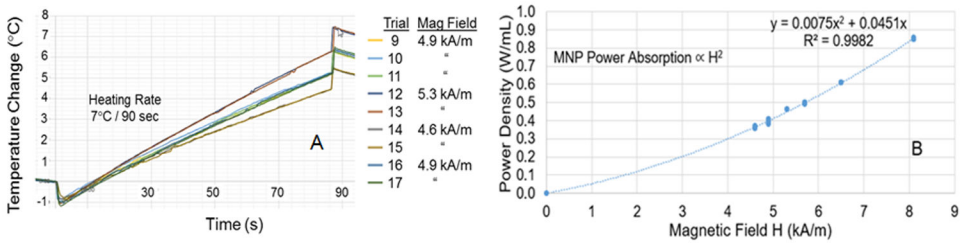

Figure 5.

Reproducibility of nanoparticle heating. (A) Heating rate of 2-cm diameter MNP-filled GliaSite® balloon in air obtained during nine independent trials at three different field strengths. (B) Power absorption in equal volume MNP-filled test chambers immersed in different magnetic field strengths repeatedly over a period of 5 months, fitted to the expected magnetic field-squared relationship (solid line).

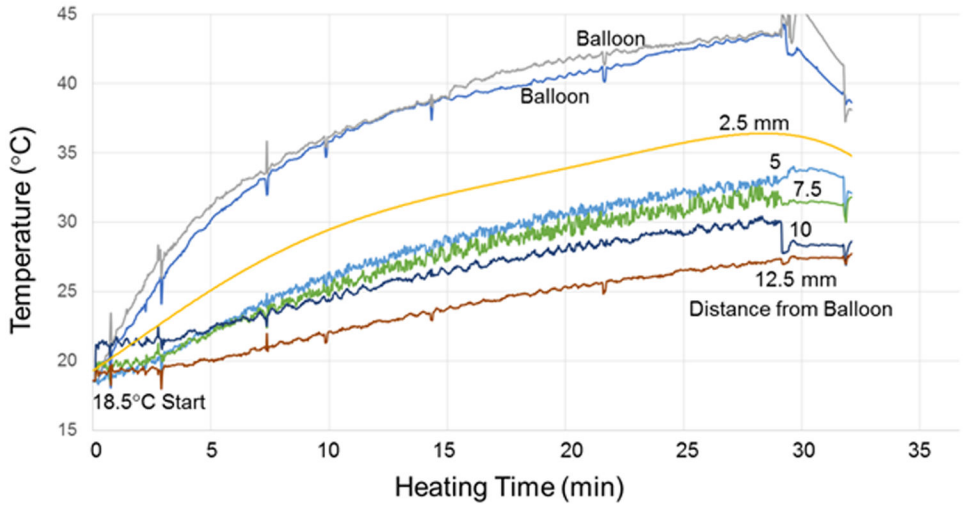

Figure 6.

Temperature rise of the MNP filled balloon surface and at 2.5, 5, 7.5, 10 and 12.5 mm radial distance in brain tissue-equivalent phantom.

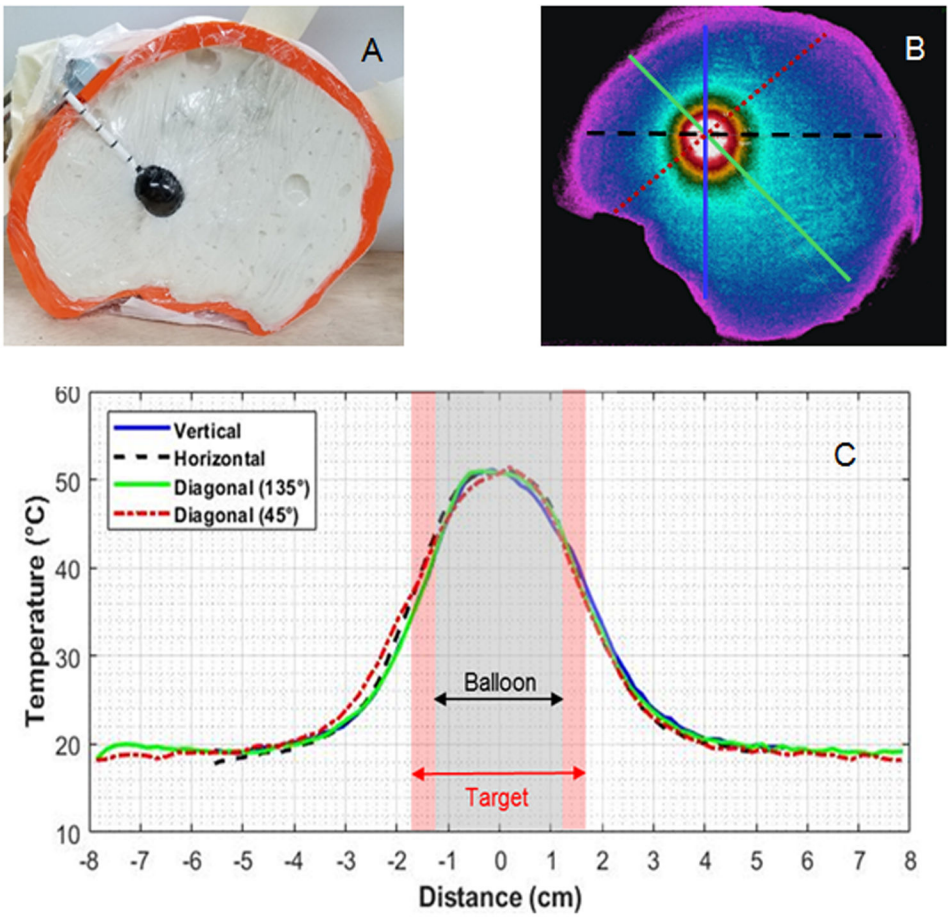

Figure 7.

(A) Human skull split-apart model filled with gelled brain tissue-equivalent phantom and 2-cm diameter magnetic nanoparticle filled balloon. (B) Thermographic camera image of the head phantom central cross-section after immersion in a magnetic field for 20 min. (C) Temperature profiles along the four radial cross-sections marked on Figure 7B demonstrate the symmetry of heating around the nanoparticle filled balloon.

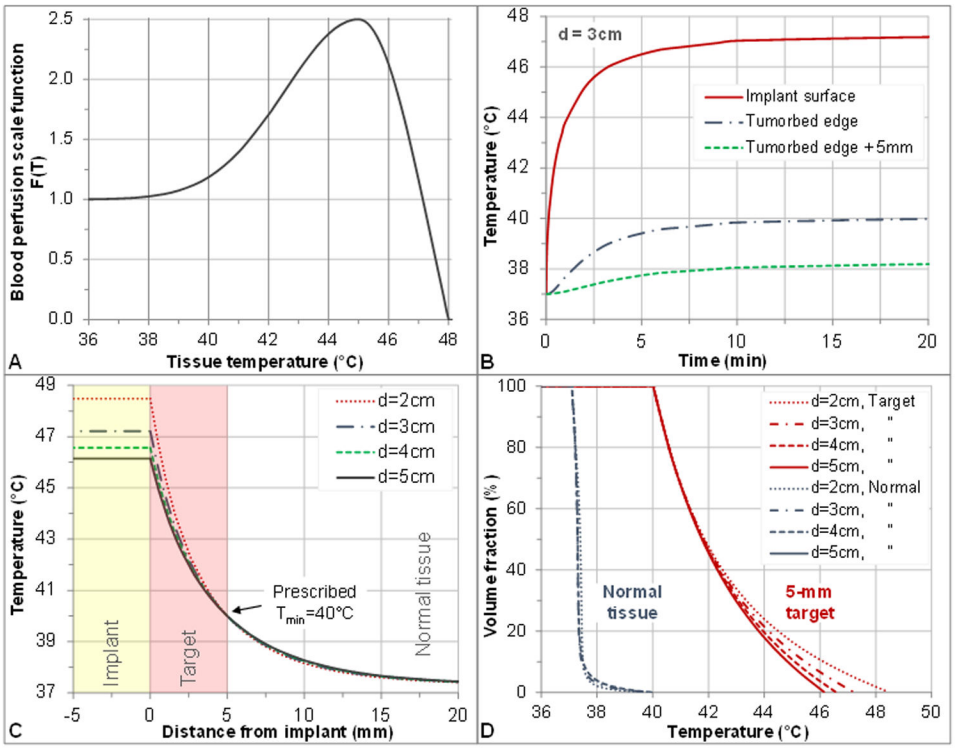

Figure 8.

Numerical simulations of MNP balloon implant heating. (A) Temperature-dependent blood perfusion scaling function F(T); (B) Simulated temperature as a function of time at the implant surface and radially 5-mm (tumor edge) and 10-mm from the surface of a 3-cm diameter balloon; (C) Simulated temperatures around 2, 3, 4, and 5 cm diameter TBT balloons implanted in tumor resection cavities in well-perfused white matter. (D) Simulated cumulative temperature-volume histograms for 2, 3, 4, and 5 cm diameter balloons heating a 5-mm annular rim target of perfused white matter. Note that for all size balloons, 100% of the 5-mm annular tumor bed target is heated above 40°C and about 50% of the target volume is heated above 41.8°C for balloon surface temperatures of 46.2 – 48.5°C.

Table 1.

Thermal and physiological properties used in the numerical simulations (42).

Property Tissue	**White matter**	**Blood**
Density, ρ (kg/m^3)	1041	1050
Specific heat capacity, **c** (J/kg/K)	3583	3617
Thermal conductivity, **k** (W/m/K)	0.48	-
Blood perfusion rate, ω_b (kg/s/m^3)	3.87	-
Metabolic heat generation rate, Q_{met} (W/m^3)	4498	-

Table 2.

Mesh settings that yield a mesh-independent solution.

	Mesh element size (mm)		Implant diameter, d (cm)
Domain	**Minimum**	**Maximum**	
Implant surface	0.026	0.5	2-5
0-5 mm from implant surface (target)	0.026	1.3	2-5
5-10 mm from implant surface	0.026	2	2-5
>10 mm from implant surface	0.195	4	2-4
	0.240	5.6	5